IEEE Access
Multidisciplinary | Rapid Review | Open Access Journal

Received December 26, 2020, accepted January 13, 2021, date of publication January 18, 2021, date of current version February 8, 2021.

Digital Object Identifier 10.1109/ACCESS.2021.3052059

Triple-Mode Microwave Filters With Arbitrary Prescribed Transmission Zeros

MUSTAFA S. BAKR, (Member, IEEE)
Institute of Pollard, University of Leeds, Leeds LS2 9JT, U.K.
Department of Physics, University of Oxford, Oxford OX1 3PJ, U.K.
e-mail: m.s.a.bakr@leeds.ac.uk; mustafa.bakr@physics.ox.ac.uk

ABSTRACT This article presents a new filter design for arbitrary placement of real frequency transmission zeros in triple-mode filters, allowing for either asymmetric or symmetric responses. Triple-mode filters can be viewed, in general, as a series combination of coupled resonators with non-adjacent couplings, allowing for the realisation of transmission zeros. The strength and phase of couplings dictate the transmission zeros locations. The arbitrary placement of transmission zeros requires controlling all amplitude and phase rations, i.e., the ability to realise both negative and positive couplings. In general, this necessitates the use of capacitive and inductive probe structures complicating the construction and hence increasing the filter cost. The method presented in this article enables arbitrary placement of transmission zeros using only inductive or only capacitive couplings structures. In addition, broadband filtering characteristics can be realised using triple-mode filters. Examples of several narrow and broadband bandpass filters are given indicating that this method is valid for most triple-mode structures.

INDEX TERMS Transmission zeros, triple-mode resonator, broadband, and bandpass filter.

I. INTRODUCTION

High performance microwave filters are key devices in many microwave systems, which are used to separate different communications signals according to their electrical frequency. The growth in wireless technology demands smaller, lighter, cheaper and faster to deploy filtering structures to meet the increasing stringent requirements both in the transmitter and receiver. Typically, high performance filters require a significant physical volume since Q factor is proportional to volume for a microwave resonator. Several approaches have been studied to overcome this problem. Dielectric resonator filters offer a dramatic reduction in size compared to metal resonators, the high permittivity results in a reduction in wavelength compared to free space. Further size reduction can be achieved by using multiple degenerate modes which increases the efficiency of volume per resonance for a given Q factor. A major advantage of multiple mode resonators is the ability to realise real-frequency transmission zeros (TZs) in in-line or cascaded configuration without the need to introduce physical cross-coupling structures [1]–[4]. Despite these advantages, the ability to individually generate and control TZs is a daunting task. In addition, multi-mode dielectric resonator filters suffers from limited bandwidth since most of the electric field is stored inside the dielectric.

The associate editor coordinating the review of this manuscript and approving it for publication was Dušan Grujić.

Triple-mode realisation of a cross-coupled network with controllable transmission zeros can be a difficult task as the TZ placements are dependent upon both the strength and phase of the couplings. The arbitrary placement of transmission zeros requires controlling all amplitude and phase rations. This requires both negative and positive couplings elements such as capacitive probes and inductive loops as well an adequate tuning mechanism where the secondary effect of frequency tuning elements is minimised. As a consequence, the filter construction complexity and cost is increased. Several papers reported the realisation of triple-mode dielectric resonator filters using non-degenerate modes [5]–[8]. However, they do not explain how to control real-frequency transmission zeros placement. Additionally, the coupling matrix (CM) reported is non-physical hindering the extraction of the full potential of filter.

This article presents a new filter design of non-degenerate triple mode dielectric resonator filters enabling arbitrary placement of transmission zeros with virtual negative or positive coupling elements while greatly simplifying the construction and thus cost of triple mode dielectric resonator filters. These new filters differ markedly from the state-of-the-art triple mode filters in the following:

1) The physical cavities may contain no coupling elements.

2) The symmetry of the structure is preserved.
3) The equivalent coupling matrix is physical.
4) The sign of coupling coefficients are altered from positive to negative and vice versa, thus flexible placement of TZs, with only inductive or only capacitive excitation ports.
5) The ability to realise broadband filters with controllable real-frequency transmission zeros.

The filter design presented is versatile and valid for most non-degenerate triple-mode dielectric resonator filters. It can be extended to multi-mode filters.

II. MODES IN TRIPLE-MODE DIELECTRIC RESONATOR FILTERS

Field plots provide useful information when selecting the coupling device suited to a particular mode. For example, a short electric probe would be most efficient when oriented along an electric field line and placed at a location of a strong electric field. In multiple mode resonators, in addition to the above, field plots can be used to provide a physical understanding of the structure that is useful for arriving to a circuit model that is physical. It is desirable to know the actual field in and around the dielectric resonator for each of the dominant modes with/without the presence of coupling structures so that an ad hoc physical circuit model and/or tuning techniques can be developed.

Multiple mode resonators can be classified as degenerate or non-degenerate. The modes are defined as degenerate if they resonant at the same frequency with equal amplitude. In dual-mode [7] and triply-degenerate (e.g. cubic [1]) resonators, the modes are split when a perturbation is introduced to the corners located along the symmetrical plane. The field distributions seen undergoes a natural rotating behavoiur in a 2-D-like fashion. In triple mode non-degenerate resonators, perturbations in the form of corner cuts or tuning screws are not required. The input and output coupling structures perturb the resonant modes such that the field distrubtion inside the metal cavity undergoes a set of rotation in a 3-D fashion such that the maxima and minima are not always located on the xy plane. Such behaviour will be shown in the next subsections.

A. CONCENTRIC

Let us examine the dominant modes of the triple-mode dielectric resonator reported in shown in Fig 1. The structure consists of a concentric dielectric puck resting on the base of a metal housing. The dominant resonant modes are the degenerate HE_{11} mode and the single TM_{01} mode. Fig 1 (a) shows a view of the three dimensional structure without any couplings present. The cross-sectional view of the electric field intensity patterns of the first three resonances is shown in Fig 1 (d,e and f). The field intensity of the three modes has a peak value outside the top face of the dielectric. Despite the three resonances having the same frequency, they have different amplitudes as shown in Figure 2(a). In other words, the wave impedance of the TM mode is different from the degenerate HE mode. The consequence of this is that, unlike degenerate dual and triple-mode filters, the presence of the excitation ports introduce unequal frequency pulling on the three modes. This is demonstrated in the field pattern shown in Fig 1 (g,h,i).

TABLE 1. Resonant Frequencies With/Without the Presence of I/O Loops.

No excitation	f1=2.5 GHz	f2=2.5 GHz	f3=2.5 GHz
Excitation	f1=2.45 GHz	f2=2.5 GHz	f3=2.55 GHz

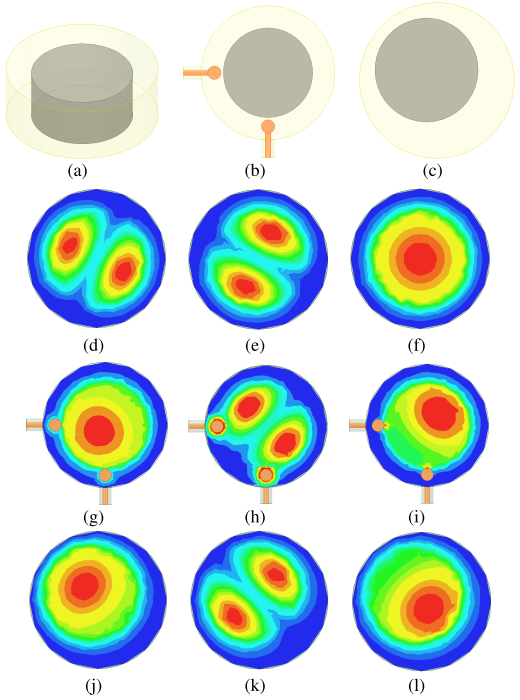

FIGURE 1. (a) 3D view of the triple-mode resonator without I/O, (b) top view with inductive I/O loops, (c) top view with a dielectric offest along the diagonal; Electric field intensity patterns of the triple-mode resonator (a) for (d) $HE11^+$ (e) $HE11^-$, (f) $TM01$; Electric field intensity patterns of the triple-mode resonator with I/O loops (b) for perturbed (g) $HE11^+$ (h) $HE11^-$, (i) $TM01$; Electric field intensity patterns of the triple-mode resonator with a dielectric offest (c) for perturbed (j) $HE11^+$ (k) $HE11^-$, (l) $TM01$.

The presence of the excitation ports blue shift and red shift the resonant frequency of the first and third modes respectively (even modes) without affecting the resonant frequency of the second mode (odd mode), equivalent to introducing a perturbation. The values of the resonant frequencies with/without the presence of the input/output ports are recorded in Table 1. Furthermore, we can observe that the perturbed field distribution of the first and third resonances undergoes a set of rotation in a 3-D fashion such that the maxima and minima are not located on the xy plane. Fig 2 shows the azimuthal electric fields of the degenerate HE and single TM modes with/without excitation ports. It is interesting to observe that the first and third mode undergoes rotations in 3D fashion such that they become degenerate. The amplitude of the second resonance remains unaffected. However, it undergoes a rotation in the transverse plane such that peak value migrates to the corner of least inductance. We can therefore assume the following:

1) The presence of the input/output probes perturbs the modes in a way similar to introducing a corner cut in degenerate dual- and triple-mode filters.

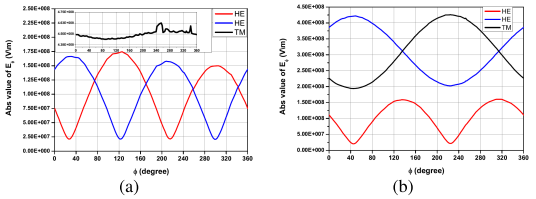

FIGURE 2. Perturbed azimuthal electric field components for $HE11^{+}$ (red), $HE11^{-}$ (blue), and $TM01$ (black) for the triple-mode resonator (a) without the presence of I/O loops, (b) with the presence of I/O loops.

2) The input/output probes excite the three modes with different amplitude and phase.
3) Couplings between the three resonances exist.
4) The structure is symmetrical along its diagonal. Therefore, its coupling matrix may be constrained to have symmetry along its diagonal simplifying the filter design and construction.

B. OFF-CENTRE

The design of filers with arbitrary bandwidth and placement of transmission zeros requires controlling all amplitude and phase rations. In other words, the degrees of freedom needs to be equal to the number of critical turning points in-band and out-of-band. Unfortunately the trade-off preserving symmetry is the decreased freedom for transmission zeros placement and in-band bandwidth. In order to provide another degree of freedom, we examine the behaviour of triple-mode filters when the dielectric puck is off-centred. Fig 1 (c) shows a cross-sectional view of an off-centred dielectric puck in a metal enclosure. The cross-sectional view of the electric field intensity patterns of the first three resonances is shown in Fig 1 (j,k and l). Similar to introducing input/output probes, the modes are perturbed such that their field patterns undergo rotation in a 3D-fashion and introduce a degeneracy between first and third modes.

Let's examine the shift in resonance as a function of offest in the xy direction. The direction of offest in shown Figure 3 for a dielectric resonator without the presence of input/output probes (a), with the presence of capacitive input/output probes (b), and with the presence of inductive input/output probes (c). The sequential coupling bandwidth between the three resonances is shown in Fig 4. Note that $K_{12} = K_{23}$ due to symmetry. The curve shows that the amount of coupling between the three resonances varies with the lateral distance between the resonator and the metal walls. By bringing the metal enclosure close to the dielectric resonator, the resonant frequency of the TM01 mode and $HE11^{+}$ are modified from the value given by the unperturbed case to a new, increased or decreased value.

The reason for such behavir can be found in the cavity perturbation theory. Namely, when a metal wall of a resonant cavity is moved inward, the resonant frequency will descrease if the stored energy of the displaced field is predominantly electric. Otherwise, when the stored energy close two the metal wall is mostly magnetic the resonant frequency will

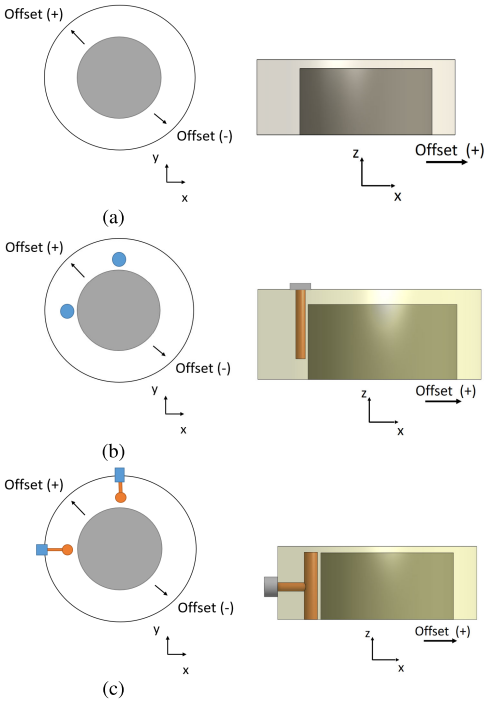

FIGURE 3. Top view and cross-sectional view of the dielectric resonator indicating the direction of offest (a) without I/O, (b) with capacitive I/O probes, and (c) with inductive I/O loops.

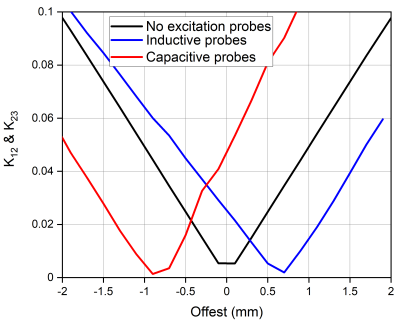

FIGURE 4. Coupling bandwidth of K_{12} as a function of offest (black curve for no I/O, blue for inductive I/O, and red for capacitive I/O).

increase when the wall moves inward. We can draw the following conclusions:

1) The lateral distance between the metal walls and the concentric dielectric puck should be kept small ($< D_{puck}$). Similarly the longitudinal distance between the top/bottom metal walls and dielectric puck may be chosen to be smaller than half the height of the puck. When the relative dielectric constant is high, e.g. around 40, most of the stored energy is located with the dielectric resonator. The remaining energy is distributed in the air around the resonator, decaying rapidly with distance away from the resonator surface. If the volume of the metal enclosure is significantly larger than the dielectric puck, the stored energy between the metal walls and dielectric puck is relatively small. Consequently, a shift of the dielectric puck toward the walls of the metal enclosure may introduce insignificant perturbation.

2) Brining the metal walls close to the dielectric resonator introduce an additional degree of freedom enabling the control of amplitude and phase ration of K_{12} and K_{S2}.

3) The lateral distance between the dielectric puck and the input/output ports is left unchanged when the metal walls moves inward or outward.

3)The amplitude of K_{12} increases remarkably as the distance between the metal walls and the dielectric puck and input/output decreases offering the possibility of realising broadband filters.

4) The sign of K_{12} changes from positive to negative in the case of inductive input/output loops and vice versa in the case of capacitive input/output probes. Thus, arbitrary placement of transmission zeros with only inductive or only capacitive input/output probes.

III. EQUIVALENT CIRCUIT

The design of triple-mode filters with arbitrary transmission zeros is based on cross-coupled circuit model and EM optimisation for the dimensional design thereafter. Typically, the final coupling matrix on which the actual filter is based on is not obtained from the extraction techniques. In other words, the objective of the similarity transformation is to force a coupling matrix to fit a realisable topology that agrees with the response of the triple-mode filter [9]. Although examining the large number of CM solutions that fits a certain reponse may seem advantageous from a flexibility design point of view, it may hinder extracting the full potential of triple-mode filters, where arbitrary placement of TZs and bandwidth is desired.

First, I explain an iterative extraction procedure of the coupling coefficients for a class of triple-mode filters preserving the structure physical properties such as symmetry. The CM is derived from the measured EM response of the filter. Second, a synthesis procedure is developed such that when transformation is applied, a unique coupling matrix exist and the solution is physical.

Typical implementation requires negative and positive couplings structures for arbitrary placements of finite transmission zeros. The approach illustrated in this section enables arbitrary placement of TZs with all negative or positive coupling structures.

A. EXTRACTION OF CHARACTERISTIC FUNCTION

The most straightforward technique is to extract the coupling matrix from the measured/simulated frequency-domain response corresponding to the physical implementation of the filter. The iterative extraction procedure is described as follows.

1) STEP 1

The group delay for a singly terminated triple-mode filter is simulated. The circuit model is extracted by adjusting the values of the phase shifter and admittance inverters until the amplitude and phase of the simulated and circuit responses agree over a wide range of frequencies. Note that in triple-mode filters, unlike single-mode filter where it is possible to remove or detune other resonators from the filter, the circuit model assumes that more than one resonator is excited in the filter. The coupling bandwidth may be extracted at this stage. The coupling coefficients between the source/load and resonators can be obtained from the group delay measurement as follows:

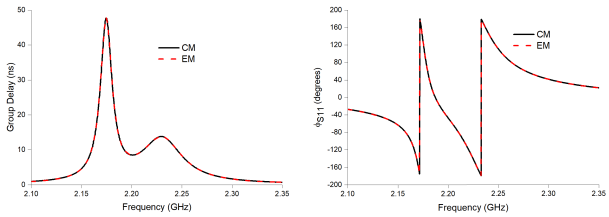

FIGURE 5. Extracted and simulated group delay (right) and phase response (left) of single terminated network.

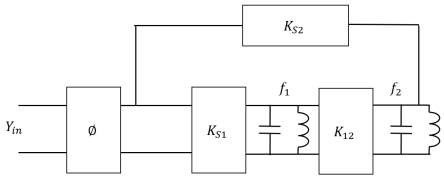

$$Qe_{Si} = \frac{2\pi f_i T_{Si}}{4}$$

$$K_{Si} = \frac{1}{Qe_{Si}}$$

The phase shifter ϕ can be equated to a π network of two shunt reactances and a series immittance inverter. The phase shift and and transmission line can be obtained after matching the group delay of the simulated/measured and circuit model response from:

$$\phi = \phi_{S11}(sim) - \phi_{S11}(circuit)$$

In the case of dispersive filters, the phase loading and transmission line are removed by curve fitting of the phase response of reflection characteristics over a wide range of frequencies. The mathematical basis for extracting the phase loading and transmission line for a measured/simulated narrowband filter is discussed in [10], [11].

The coupling bandwidth between the even and odd resonances (mainline couplings) is obtained as follows:

$$K_{12} = \frac{f_e^2 - f_o^2}{f_e^2 + f_o^2}$$

As an example, the structure in Figure 1(b) is simulated and the extracted couplings are shown below.

2) STEP 2

The second terminal is added and the filter is re-simulated. The phase-corrected S-parameters are converted to Y-parameters for rational approximation and extraction of the coupling matrix. The coupling coefficients obtained from step 2 are kept unchanged and the remaining unknown

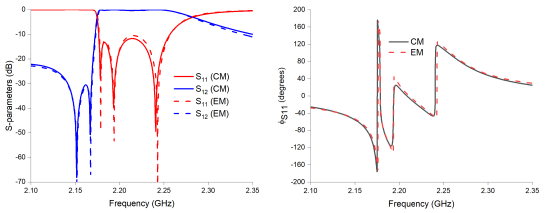

FIGURE 6. Extracted and simulated magnitude and phase of the triple-mode filter shown in Figure 1 (b).

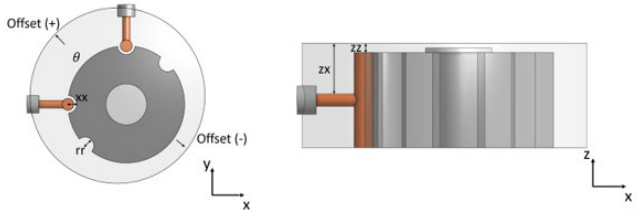

FIGURE 7. Top view (left) and cross-sectional view (right) of triple-mode filter with offest in the (-) direction.

coupling coefficients are adjusted until the amplitude and phase responses for the coupling matrix and EM simulated closely in agreement. The constrain added is that the CM is symmetric along its diagonal.

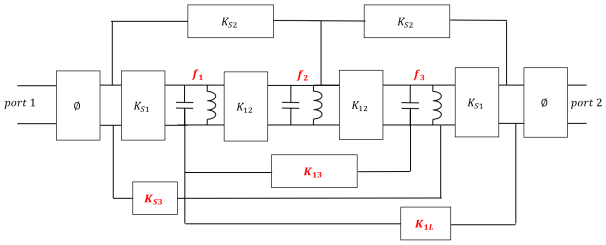

3) STEP 3

All coupling coefficients of the constrained CM are adjusted until the two responses agree well.

$$M = \begin{bmatrix} 0 & 0.719 & -0.374 & 0.019 & 0 \\ 0.719 & 0.269 & 0.512 & 0.047 & 0.019 \\ 0.374 & 0.512 & -0.782 & 0.5121 & 0.374 \\ 0.019 & 0.047 & 0.512 & 0.313 & 0.719 \\ 0 & 0.019 & -0.374 & 0.719 & 0 \end{bmatrix}$$

B. SYNTHESIS

The synthesis procedure starts with the classical transversal coupling matrix obtained from the transfer and reflection polynomials [12]. The synthesised coupling matrix is then reconfigured with a sequence of similarity transformation [13]. The similarity transform is constrained in which symmetry is preserved. The following system of equations is solved yielding a unique solution:

$$\begin{aligned} M^1 &= PM_0P^t \\ PP^t &= I \\ M^1_{ij} &= 0 \quad \forall ij \in A1 \\ M^1_{ij} &= M^1_{kl} \quad \forall ij \text{ and } kl \in A2 \end{aligned}$$

$$M = \begin{bmatrix} M_{SS} & M_{S1} & M_{S2} & M_{S3} & M_{SL} \\ M_{S1} & M_{11} & M_{12} & M_{13} & M_{S3} \\ M_{S2} & M_{12} & M_{22} & M_{12} & M_{S2} \\ M_{S3} & M_{13} & M_{12} & M_{33} & M_{S1} \\ M_{SL} & M_{S3} & M_{S2} & M_{S1} & M_{LL} \end{bmatrix}$$

For this configuration only one real solution exists which is physical and are therefore of practical interest.

C. PHYSICAL DIMENSIONING

The aim of synthesis is to develop an effective design recipe and establish a linkage between the equivalent circuit and the physical dimensions of the structure. The next step in the synthesis process is to introduce a relation between the coupling values in the physical CM and the dimensions of the filter. For the loaded dielectric waveguide filter in Figure 7, the mainline couplings and non-sequential couplings are realised as inductive loops. At first glance, it may seem very challenging to assign the couplings obtained to physical dimensions as nearly all couplings depend to some degree on the dimensions of the inductive loops. Unlike single-mode filters where electromagnetic techniques may be sufficient to assign a one-to-one relation between couplings and physical dimensions, triple-mode filters may not have a direct linkage between the couplings values and physical dimensions. Instead, the extraction procedure described earlier coupled with electromagnetic techniques may be used to understand the relation between each physical dimensions and the couplings assigned it. In order to do that, a physical CM is required. For example, the couplings coefficients as a function of the offest of the dielectric puck as well as the tapping point of the transformer is shown in Figure 8. We can observe that varying the distance between the metal walls and the dielectric puck mainly adjusts the amplitude and phase of M_{12} and M_{S2}. On the other hand, varying the height zx (figure 8) mainly adjust the amplitude of M_{S1}. The radius and position of the longitudinal grooves mainly adjust the coupling value and sign of M_{13} respectively. A fully canonical response, where the number of transmission zeros equal N, can be obtained by varying the angle between the I/O ports (non-90 deg.) which results in a direct coupling between source and load. The location of TZs can be controlled by adjusting the strength and sign of coupling values between adjacent and non-adjacent nodes. For example, altering the sign of M_{S2} and M_{13} will shift the location of TZs from the low-side to the high-side of the passband. The extraction process described above is repeated for every physical dimensions and the dependency of each coupling is derived as shown in Table 2. Lookup tables can be produced and then used for physical dimensioning of higher order filters with arbitrary bandwidth and placement of transmission zeros. A tuning mechanism can be derived from the data obtained from the extraction process to account for the primary and secondary tuning effects and meet stringent specification. Thus, a triple-mode

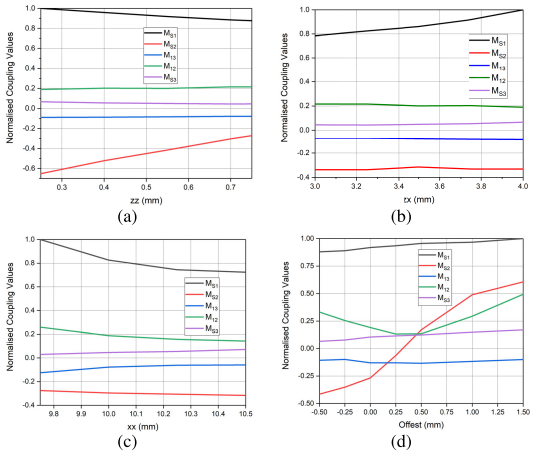

FIGURE 8. Coupling coefficients versus (a) gap between inductive loop and cavity lid (b) dimensions of probe tapping height (c) gap between inductive loop and dielectric puck (d) resonator offset.

TABLE 2. Primary and Secondary Effect of Each Physical Dimension on the Coupling Coefficients.

Physical dimensions	Primary effect	Secondary effect
zz	M_{S2}	M_{S1}
zx	M_{S1}	-
xx	M_{S1}, M_{12}	M_{S2}
Offest (+/-)	M_{12}, M_{S2}	M_{S1}
rr	M_{13}	M_{12}
θ (angle between I/O)	M_{S1}, M_{S3}, M_{12}	M_{SL}, M_{S2}, M_{13}

TABLE 3. Physical Dimensions.

zz=1.05mm	zx=5.6mm	xx=0.6mm
Offest (+)=1.75mm	rr=1.5mm	θ=90 deg.

TABLE 4. Comparison With Other Reported Triple-Mode Filters.

Ref.	this work	1	8
f_0	2.45GHz and 2GHz	1.85GHz	1.5GHz
$IL(dB)$	0.16 and 0.18	0.3	0.43
FBW	3.4% and 6.8%	4%	1%.
TZs	controllable and tunable post fabrication (N-1)	controllable and non-tunable post-fabrication (N)	not controllable (N-1).

filter with truly arbitrary location of transmission zeros can be designed (Table 4).

IV. DESIGN EXAMPLES

A. BANDPASS FILTERS WITH TRANSMISSION ZEROS ON THE HIGH SIDE

Let's us consider a filter with the following specifications:
Passband: 2.417-2501 GHz; Return Loss: 20 dB.
Stopband: 2.517-2.654 GHz; Isolation $<$ 23 dB.

Here, a Generalised Chebyshev bandpass characteristic of third order with two transmission zeros on the high side is required. The synthesis procedure yields the following

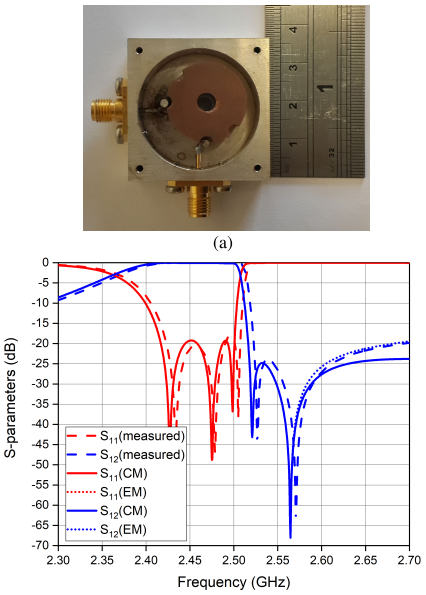

FIGURE 9. (a) Photograph of the triple-mode filter with offest in the (-) direction. (b) Responses of the triple mode filter by CM (solid lines), simulation (dotted lines), and measured (dashed lines).

physical CM:

$$M = \begin{bmatrix} 0 & 1.013 & 0.320 & 0.086 & 0 \\ 1.013 & -0.343 & 0.952 & 0.419 & 0.086 \\ 0.320 & 0.952 & 0.0969 & 0.952 & 0.320 \\ 0.086 & 0.419 & 0.952 & -0.317 & 1.013 \\ 0 & 0.086 & 0.320 & 1.013 & 0 \end{bmatrix}$$

The implementation of the CM exploits the triple-mode filter in Figure 7. As explained in section III (A) and shown in Figure 6, a triple-mode filter with concentric dielectric puck and inductive input/output loops produces a bandpass filter with two transmission zeros on the low side. The realisation of transmission zeros on the high side requires capacitive input/output probes as reported in [6]. However, this may not be desired due to bandwidth, complexity and cost limitation. Figure 7 shows a sketch of the triple-mode filter with inductive input/output loops and an offest in the (+) direction. As seen in Figure 4 and 8, an offest in the (+) direction alters the sign of M_{S2} from (-) to (+) without the need to use capacitive input/output probes. It also offers control of amplitude and phase ratio of M_{12}. The amplitude and sign of M_{13} is dominantly controlled by location and radius of the corner cuts along the diagonals (rr). Note that the structure in Figure 7 is symmetric along the diagonal. The diameter and height of the metal cavity and dielectric puck is obtained from an electromagnetic simulator $H_{cavity} = 11.4mm$, $H_{puck} = 10mm$, $D_{cavity} = 30mm$, and $D_{puck} = 20mm$. The dimensions of the input/output couplings and offest needed to meet the specification are to obtained from the lookup tables produced from the extraction techniques described earlier yielding: The fabricated device, and the simulated and measured responses are shown in Figure 9, showing good agreement. To validate the statement that the obtained coupling matrix is physical, the extraction procedure is repeated for Figure 7. The results

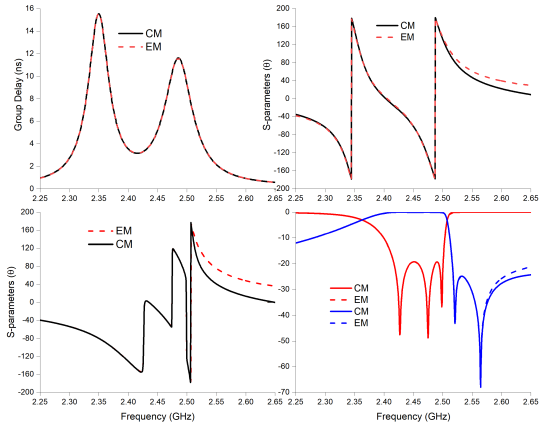

FIGURE 10. Extracted and simulated amplitude and phase response of the triple-mode filter in Figure 7.

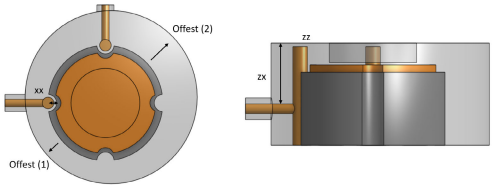

FIGURE 11. Top view (left) and cross-sectional view (right) of triple-mode filter with offest in the (1) direction.

obtained are shown in Figure 12, showing a good agreement between theory and design.

B. BROADBAND BANDPASS FILTERS WITH TRANSMISSION ZEROS ON BOTH SIDE

Let's us consider a broadband filter having a symmetric response with the following specifications:
Passband: 1.927-2.0603 GHz; Return Loss: 20 dB.
Stopband: 1.7-1.87 GHz and 2.13-2.4 GHz; Isolation $<$ 19 dB.

Here, a Generalised Chebyshev bandpass characteristic of third order with transmission zeros on both sides is required. The fractional bandwidth (%) is 6.8. The synthesis procedure yields the following CM:

$$M = \begin{bmatrix} 0 & 0.828 & -0.615 & 0.0509 & 0 \\ 0.828 & 1.073 & 0.6123 & -0.112 & 0.1016 \\ -0.615 & 0.6123 & 0.1383 & 0.6123 & 0.574 \\ 0.0509 & -0.112 & 0.6123 & -0.764 & 0.828 \\ 0 & 0.1016 & 0.574 & 0.828 & 0 \end{bmatrix}$$

The implementation of the CM exploits the triple-mode filter in Figure 11. The height of the metal enclosure is reduced to redshift the resonant frequency of TM_{01} mode and form a triple resonance combined with the degenerate TM_{11}-like modes. The input/output couplings structures as realised as inductive loops. The dielectric puck is offest in the direction "offest(1)" in Figure 11(b). The consequence of this is to alter the sign of coupling of M_{S2} such that $M_{L2} = -M_{S2}$ and thus, moving a transmission zero of the low to the high side resulting in symmetric response (transmission zeros on both side). The circuit and EM simulated responses are shown in Figure 12.

TABLE 5. Various Implementation of Triple-Mode Filters With Asymmetric and Symmetric.

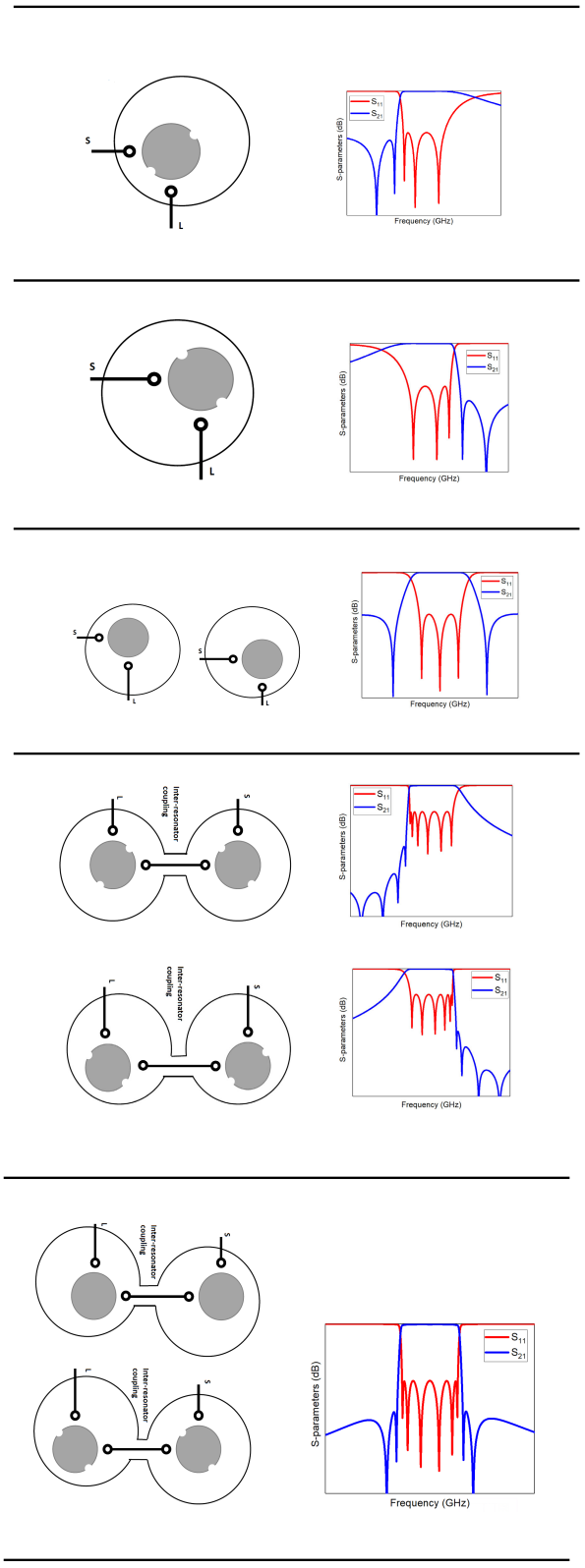

TABLE 5. *(Continued.)* **Various Implementation of Triple-Mode Filters With Asymmetric and Symmetric.**

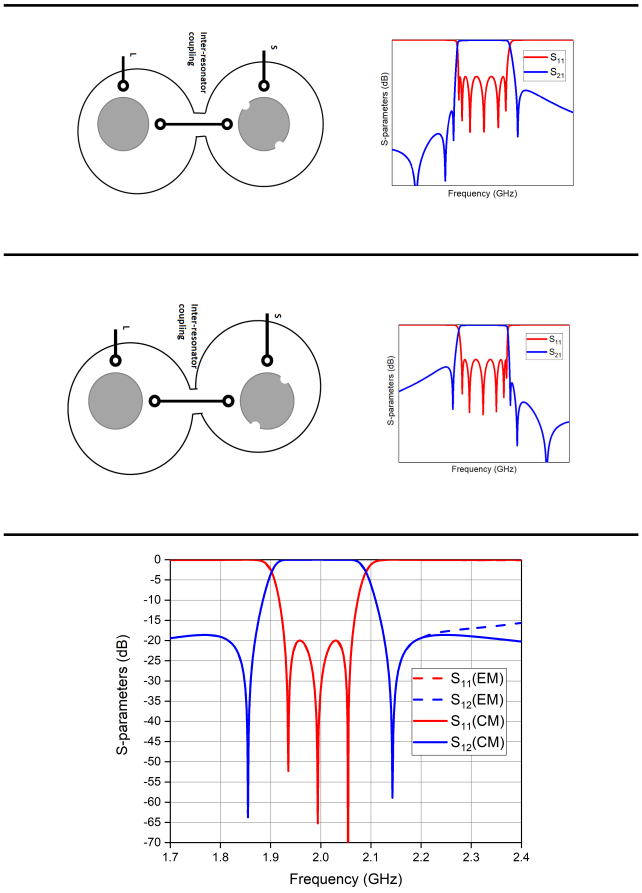

FIGURE 12. **Theoretical and simulated responses of a three-pole bandpass filter with transmission zeros on both sides.**

C. IMPLEMENTATION OF OFF-CENTRED TRIPLE-MODE FILTERS WITH SYMMETRIC/ASYMMETRIC RESPONSES

The design examples presented above aimed to show the versatility and potential of the design procedure explained and the flexibility introduced by offest the dielectric puck while maintaining symmetry. The same procedure may be followed for the design of off-centred triple-mode filters using capacitive input/output couplings. The different implementation of triple-mode filters using inductive input/output loops with symmetric and asymmetric responses are shown in Table 5. A comparison between the proposed filter design and several reported triple-mode filters, where the merits of this article about arbitrary prescribed transmission zeros with simplified structures, is shown in Table 4.

V. CONCLUSION

In this article, a new design procedure for non-degenerate triple-mode filter was introduced. The representation of filters using a physical coupling matrix that is extracted from extraction techniques enables the design of filters with arbitrary placement of transmission zeros and bandwidth. Off-centred dielectric resonators offers an extra degrees of freedom enabling flexible placement of transmission zeros and the realisation of broadband filters with only inductive or capacitive coupling structures. Design examples of symmetric and asymmetric narrowband and broadband filters were shows demonstrating the versatility of the proposed filter design.

REFERENCES

[1] D. R. Hendry and A. M. Abbosh, "Analysis of compact triple-mode ceramic cavity filters using parallel-coupled resonators approach," *IEEE Trans. Microw. Theory Techn.*, vol. 64, no. 8, pp. 2529–2537, Aug. 2016.
[2] S. Amari and U. Rosenberg, "A circular triple-mode cavity filter with two independently controlled transmission zeros," in *Proc. Eur. Microw. Conf.*, Manchester, U.K., Sep. 2006, pp. 1091–1094.
[3] M. S. Bakr, F. Gentili, and W. Bosch, "Triple mode dielectric-loaded cavity band pass filter," in *Proc. 16th Medit. Microw. Symp. (MMS)*, Abu Dhabi, United Arab Emirates, Nov. 2016, pp. 1–3.
[4] S. Amari and U. Rosenberg, "New in-line dual-and triple-mode cavity filters with nonresonating nodes," *IEEE Trans. Microw. Theory Techn.*, vol. 53, no. 4, pp. 1272–1279, Apr. 2005.
[5] M. S. Bakr, I. C. Hunter, and W. Bosch, "Miniature triple-mode dielectric resonator filters," in *IEEE MTT-S Int. Microw. Symp. Dig.*, Philadelphia, PA, USA, Jun. 2018, pp. 1249–1252.
[6] M. S. Bakr, I. C. Hunter, and W. Bosch, "Miniature triple-mode dielectric resonator filters," *IEEE Trans. Microw. Theory Techn.*, vol. 66, no. 12, pp. 5625–5631, Dec. 2018.
[7] X.-C. Zhu, W. Hong, K. Wu, H.-J. Tang, Z.-C. Hao, J.-X. Chen, and P. Chu, "Design and implementation of a triple-mode planar filter," *IEEE Microw. Wireless Compon. Lett.*, vol. 23, no. 5, pp. 243–245, May 2013, doi: 10.1109/LMWC.2013.2253313.
[8] X. X. Yuan, L.-H. Zhou, and J.-X. Chen, "Triple-mode bandpass filter based on silver-loaded ring-shaped dielectric resonator," *IEEE Microw. Wireless Compon. Lett.*, vol. 28, no. 9, pp. 789–791, Sep. 2018, doi: 10.1109/LMWC.2018.2853568.
[9] S. Amari, "Application of representation theory to dual-mode microwave bandpass filters," *IEEE Trans. Microw. Theory Techn.*, vol. 57, no. 2, pp. 430–441, Feb. 2009.
[10] Y. Zhang, H. Meng, and K.-L. Wu, "Direct synthesis and design of dispersive waveguide bandpass filters," *IEEE Trans. Microw. Theory Techn.*, vol. 68, no. 5, pp. 1678–1687, May 2020, doi: 10.1109/TMTT.2020.2969385.
[11] P. Zhao and K.-L. Wu, "Model-based vector-fitting method for circuit model extraction of coupled-resonator diplexers," *IEEE Trans. Microw. Theory Techn.*, vol. 64, no. 6, pp. 1787–1797, Jun. 2016, doi: 10.1109/TMTT.2016.2558639.
[12] R. J. Cameron, J.-C. Faugere, F. Rouillier, and F. Seyfert, "Exhaustive approach to the coupling matrix synthesis problem and application to the design of high degree asymmetric filters," *Int. J. RF Microw. Comput.-Aided Eng.*, vol. 17, no. 1, pp. 4–12, Jan. 2007.
[13] R. J. Cameron, C. M. Kudsia, and R. R. Mansour, *Microwave Filters for Communication Systems*. Hoboken, NJ, USA: Wiley, 2007.

MUSTAFA S. BAKR (Member, IEEE) received the B.Sc. degree (Hons.) from the University of Technology, Baghdad, Iraq, in 2012, the M.Sc. degree (Hons.) from the University of Leeds, Leeds, U.K., in 2015, and the Ph.D. degree (Hons.) from the Graz University of Technology, Graz, Austria, in 2018. He is currently with the Department of Physics, University of Oxford, U.K. He is also with the Institute of Pollard, University of Leeds, U.K. He has authored or coauthored several articles and a book chapter. He has six patents. His current research interests include superconducting quantum circuits, microwave filters and antennas for the IoT, and mobile communication.

Dr. Bakr is a Fellow of the Higher Education Academy, U.K., and a member of IET. He was a recipient of the IEEE MTT-S Graduate Fellowship Award for the year 2017, Erasmus Grant, from 2016 to 2017, the Best Poster Award at EWSN2017, and the Best Demo Award at SenSys 2017.